Structural Determination of a Carbocation-Derived Rearrangement Product Observed During Thiele Cage Opening: Insight into the mechanism of an alkyl-extended pinacol reaction

A. L. Burman, J. K. Sader & J. E. Wulff

2024

Structural Determination of a Carbocation-Derived Rearrangement Product Observed During Thiele Cage Opening: Insight Into the Mechanism of an Alkyl-Extended Pinacol Reaction

Austin L. Burman, Jonathan K. Sader and Jeremy E. Wulff*

Department of Chemistry, University of Victoria, PO Box 065 STN CSC, Victoria, BC V8W 3V6, Canada

E-mail: wulff@uvic.ca

Abstract

A substituted bishomocubane structure colloquially known as a Thiele cage was previously observed to undergo an alkyl-extended pinacol-type rearrangement, wherein 1,2-aryl migration and ketone formation occurred together with (or at least in close succession to) opening of a strained cyclobutane bond. While there was some indication that the rearrangement reaction might proceed *via* a stepwise process involving a sequence of carbocation intermediates, previous studies did not uncover any direct evidence for the formation of carbocations, and did not fully explain the regio- and stereospecificity of the reaction. Here we describe the isolation and detailed characterization of a second rearrangement product formed under the pinacol reaction conditions, the existence of which implicates the formation of discrete carbocation intermediates along the reaction pathway. Observation of this new product also finally explains the fate of any Thiele cage material that is converted to a carbocation, but which is not geometrically predisposed to react through a facile 1,2-aryl migration. As such, our findings resolve previous questions surrounding the origin of regio- and stereospecificity in the alkyl-extended pinacol rearrangement.

Key words: pinacol rearrangement, Thiele cage, structural characterization, NMR

Introduction

Pinacol rearrangements[1,2] provide a versatile means of skeletal reorganization within organic molecules, and have been extensively employed in complex molecule synthesis.[3–10] The reaction, which can be either concerted or stepwise (in which case an intermediate carbocation is formed), proceeds through cleavage of a C–C bond in

a vicinal diol, together with concomitant 1,2-migration of an alkyl or aryl group (Scheme 1A). π-Extended variants of the pinacol rearrangement, in which an additional sp^2–sp^2 C=C bond is present between the two alcohol groups of the starting material, are also well known,[11–14] and have been exploited in asymmetric synthesis.[14] By contrast, alkyl-extended pinacol reactions, in which the leaving group and the migrating group are separated by an additional sp^3–sp^3 C–C bond, were largely unknown prior to 2019. A single example of a cyclopropane-extended pinacol rearrangement was reported by Darby and Lutz (Scheme 1B),[15] but since the sp^5 hybridization state of the cyclopropane carbon atoms contributes significant π character to the bond being cleaved, this does not constitute a true alkyl-extended pinacol rearrangement.

In 2019, our group reported what we believe to be the first extended pinacol reaction to occur across an sp^3–sp^3 bond.[16] The reaction takes place within a strained bishomocubane (**1**; Scheme 1C) that is functionalized with four aryl groups, and which is readily accessible through Diels–Alder dimerization of carboxylated cyclopentadiene[17–20] followed by photochemically promoted intramolecular [2+2] cycloaddition to close the cage structure[21–25] and then four-fold addition of an aryl lithium reagent. The initially formed Diels–Alder dimer is known as Thiele's ester (or Thiele's acid for the corresponding *bis*-carboxylic acid[21,26,27]), and so by analogy the bishomocubane cycloaddition product is referred to as a Thiele cage.[16]

One interesting—and not yet well understood—feature of the alkyl-extended pinacol rearrangement shown in Scheme 1C is the apparent regio- and stereospecificity of the reaction. Only one of the four aryl groups present on substrate **1** undergoes migration, leading to a single isomer of product. We initially wondered if the specificity of the rearrangement reaction might be due to the existence of a concerted transition state, since the competing stepwise mechanism (Scheme 2) would seem likely to generate a mixture of diastereomers and regioisomers (i.e. **2**, **3**, **4**, and **5**) but only one of these products could be detected within the crude reaction mixture. However, subsequent study revealed that an electron-rich substrate (**2b**) reacted much more quickly than the parent arene (**2a**), while an electron-poor congener (**2c**) barely reacted at all.[16] These data suggested the intermediacy of a pair of interconverting benzylic carbocations (**I** and **II**; Scheme 2), which would be

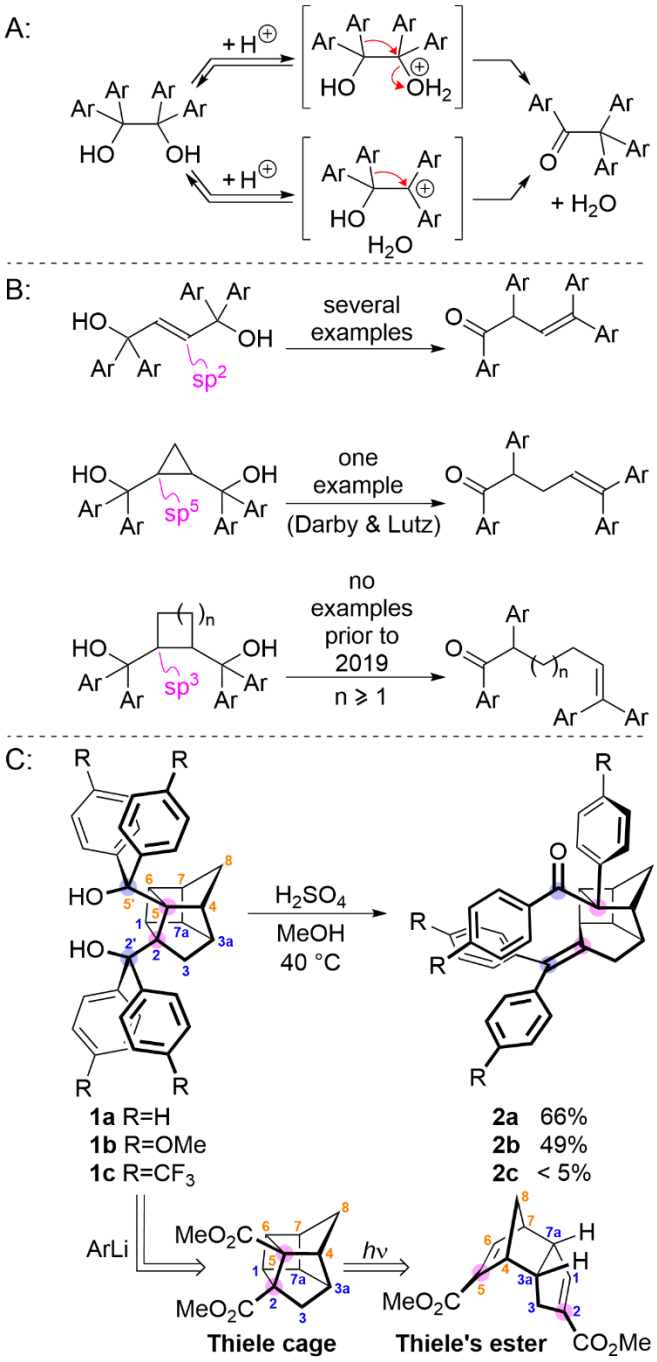

46

47 **Scheme 1.** Pinacol rearrangements and π- or σ-extended variants. **A:** The classic pinacol rearrangement, which
48 can proceed *via* concerted or stepwise mechanisms. **B:** Extended pinacol rearrangements. **C:** Thiele cage
49 opening, proceeding *via* extended pinacol rearrangement across an sp^3–sp^3 bond.

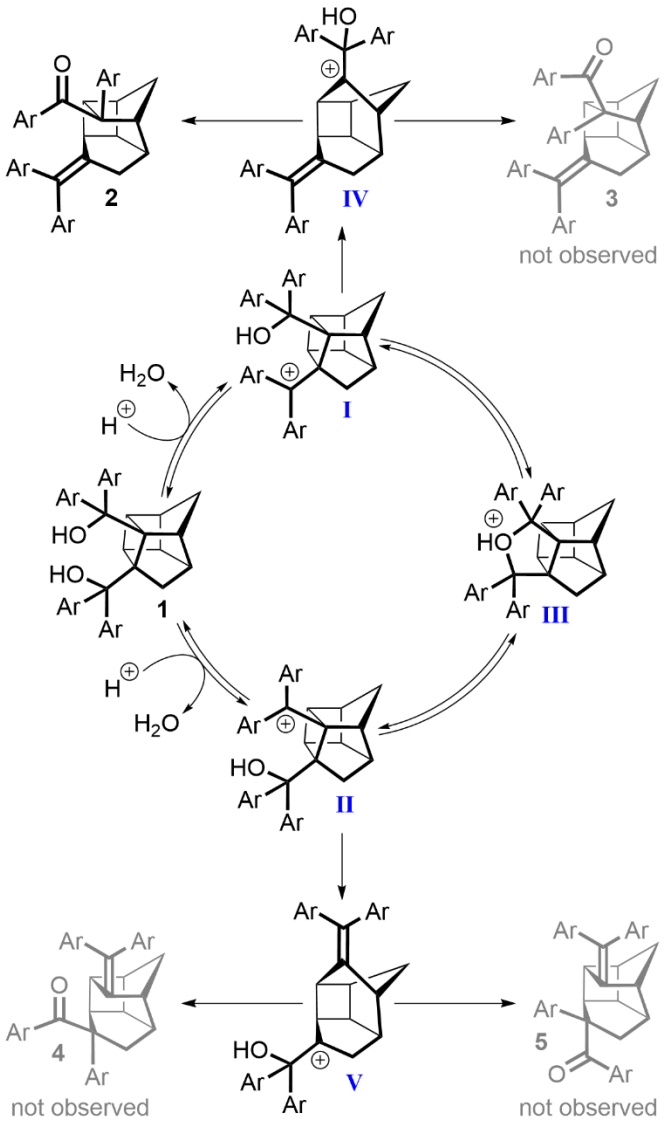

Scheme 2. Possible stepwise mechanism accounting for the extended pinacol rearrangement of diol **1**.

stabilized by the electron-donating methoxy group in **2b**, and destabilized by the *para*-CF_3 group in **2c**. If this were the case, however, then why did these intermediate carbocations not give rise to all four possible isomeric products (**2**–**5**)? Indeed, preliminary DFT calculations on the relative energetics and conformational preferences of cations **IV** and **V** (which would result from opening of the cyclobutane rings in **I** and **II** and whose formation would likely not be reversible under the conditions of the reaction, given the significant release of ring-strain involved) gave little indication of why the reaction should exhibit any significant preference for the formation of ketone **2** over **3**, **4**, or **5**.[16]

A partial answer to this question came from solving an X-ray structure for **1a** (Figure 1).[16] The crystal structure data revealed a distinct lengthening of the C2–C5 bond in diol **1** (1.66 Å vs. 1.56 Å for the other six cyclobutane bonds present in the structure), and also clearly showed that one (and only one) of the four arene groups was positioned in an almost perfectly antiperiplanar orientation ($\theta_{(C19\text{-}C5'\text{-}C5\text{-}C2)}$ = 177.04(8)°) relative to the weakened bond. In other words, the preferred conformation of **1** is primed to favour the production of **2** over any other pinacol rearrangement products. Provided that the intermediate carbocations (particularly **IV**) are sufficiently short-lived that they cannot equilibrate to their own preferred geometry, the conformational preferences of compound **1** visible in the X-ray structure may help to explain preferred formation of ketone **2**.

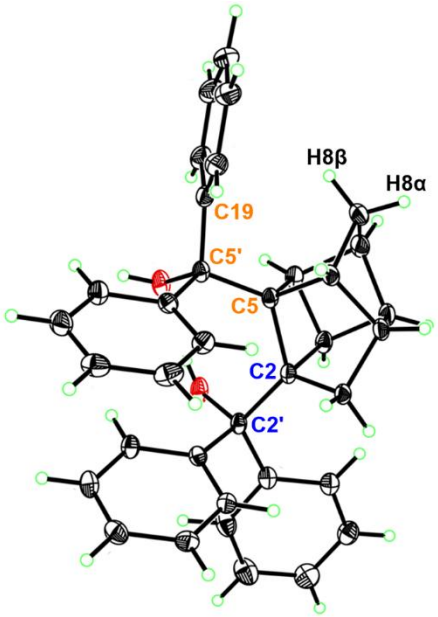

Figure 1. X-ray structure of **1a**, revealing a lengthening of the C2–C5 bond and a positioning of one of four aryl groups antiperiplanar to the bond that is broken during the extended pinacol rearrangement. H8ß comes into resonance at –0.64ppm in the ^{1}H NMR spectrum, suggesting that the preferred solution-state conformation is similar to what is visible in the solid-state.

One must always be cautious in using solid-state structures to rationalize solution-state reactivity, but in this case we had at least one piece of evidence supporting the notion that the X-ray structure was broadly similar to that of the preferred solution-state conformation for **1a**. In the solid-state structure, we observed that the ß-

proton at H8 was pushed into the face of the migrating aryl ring. This should result in a pronounced magnetic shielding effect for this proton, and indeed in the solution-state ^{1}H NMR we found that H8ß came into resonance at –0.64 ppm.

The structural properties of **1a** provided some explanation as to why **2** would be favoured over **3**, but still left two lingering concerns. First, we had no direct evidence for the formation of a carbocation intermediate in the reaction mechanism leading from **1**. Second, it seemed likely that any reaction that formed cation **IV** would also form at least some of cation **V**, since the two species were of similar structure and had similar energy. Since **V** seemed unlikely to enter the reaction manifold by conversion back to **II** due to the increasing ring strain involved in such a transformation, we were puzzled by what might become of any material that passed *through* intermediate **V**, given that no signals suggestive of **4** or **5** were ever observed in the crude NMR spectra.

Here we describe the isolation and characterization of a secondary rearrangement product from **1**, which forms under similar conditions to that of **2**, and whose formation clearly proceeds through a series of carbocation intermediates—providing compelling evidence that the pinacol rearrangement pathway can access similar cationic intermediates along the reactivity landscape. Furthermore, the reaction pathway leading to this new product provides a shunt to account for the material that passes through intermediate **V**. In this way, the observation of the new rearrangement product resolves the two mechanistic concerns identified above.

Results and Discussion

During our initial study of the conversion of **1a** to **2a**, we had observed the simultaneous formation of a low-yielding side product, **6a**. The ^{1}H and ^{13}C NMR spectra for **6a** were inconsistent with isomers of **2a** (e.g. **3**, **4**, or **5**) but we were unable to determine its precise structure because of extensive overlap in the aromatic region of the ^{1}H NMR spectrum (Figure 2A)—although the aliphatic region was nicely resolved (Figure 2B). We reasoned that the use of a structural analogue of **1a** in which *para*-substituted aromatic rings were incorporated would lead to an analogous side product with a better-resolved NMR spectrum. Unfortunately neither **1b** nor **1c** afforded the corresponding minor product in sufficient yield or purity to permit characterization. We therefore

synthesized diol analogue **1d** (Scheme 3) in which four *para*-tolyl groups were incorporated into the structure. As expected, **1d** rearranged similarly to **1a**, affording the expected extended pinacol product (**2d**) in good yield, alongside a minor product (**6d**) that was clearly related to the previously obtained **6a**. Gratifyingly, the downfield region of the ^{1}H NMR spectrum for **6d** was cleanly resolved (Figure 3A), although unfortunately the upfield region suffered from extensive overlap of signals (Figure 3B). In this way, the NMR spectra for **6a** and **6d** were complementary to one another; the parts of the spectra that were uninterpretable for **6a** were clearly resolved for **6d**, and *vice versa*. We therefore undertook to determine the correct structure of our mystery side product, using data from a series of 1D and 2D NMR experiments (1D ^{1}H and ^{13}C, 1D NOE, COSY, HSQC and HMBC) conducted simultaneously on both molecules.

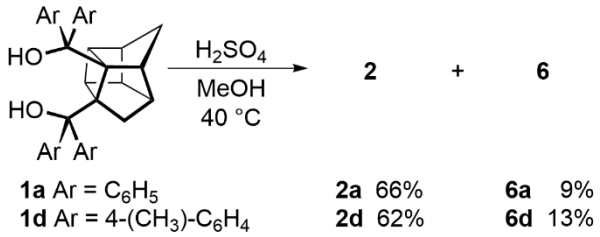

Scheme 3. Synthesis of an analogue amenable to NMR studies.

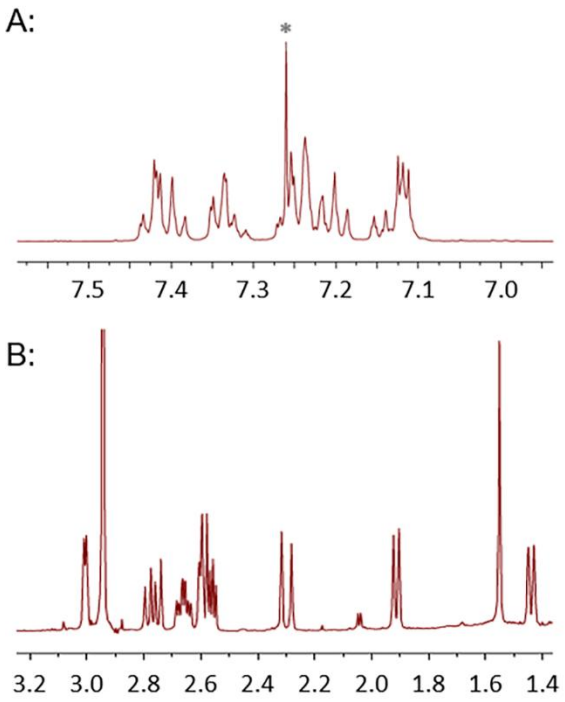

117

118 **Figure 2.** ^{1}H NMR spectrum for **6a** in $CDCl_3$. **A:** Aromatic region. **B:** Aliphatic region. *Residual $CHCl_3$ in the NMR
119 solvent. Axis labels are in ppm.

120

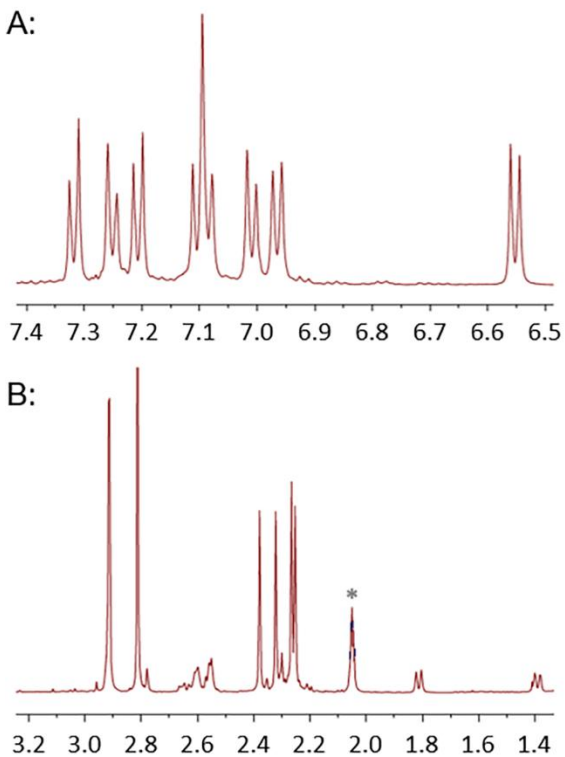

121

122 **Figure 3.** ^{1}H NMR spectrum for **6d** in acetone-d6. **A:** Aromatic region. **B:** Aliphatic region. *Residual $CD_3C(O)CD_2H$
123 in the NMR solvent. Axis labels are in ppm.

124

The well-resolved aromatic region of the ^{1}H NMR spectrum for **6d** allowed us to distinguish the four separate spin systems for the four aromatic rings in the product. This in turn allowed for a series of HMBC experiments (Figure 4), which conclusively showed that two aryl rings (arbitrarily labeled A and B) were connected to a single carbon atom (C2') while the other two aryl rings (C and D) were likewise connected to a single carbon atom (C5'). Particularly diagnostic HMBC correlations were observed from *ortho* protons H16 and H12 to C2' and from *ortho* protons H24 and H20 to C5' (refer to Figure 4 for atom numbering; protons H12, H16, H20, and H24 were established as being *meta* to the tolyl methyl groups in **6d** through analysis of the COSY and HMBC spectra). C2' and C5' were identified as fully substituted vinyl carbons due their chemical shifts (137.20 and 138.40 ppm in the ^{13}C NMR spectrum), together with the absence of a signal in the DEPT-135 spectra and a lack of HMBC correlation to the tolyl CH_3 resonance.[28] The two carbons on the other end of the alkenes (i.e. C2 and C5) were likewise found to be fully-substituted, through an absence of signal in the DEPT-135 spectra. In summary, then, we were able to establish the presence of two very hindered 1,1-diarylalkene fragments within **6d** and (due to similar ^{13}C resonances) **6a**. From a mechanistic perspective, the connectivity of these tetrasubstituted alkenes implied elimination of both hydroxyl group in **1**, without the concomitant 1,2-migration of an aryl group.

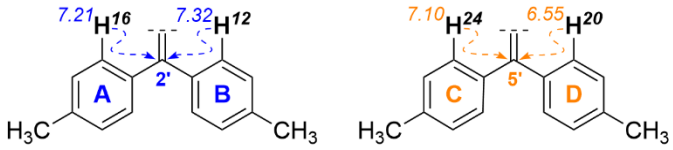

Figure 4. HMBC interactions in **6d**, establishing connectivity in the two 1,1-diarylalkene fragments within the molecule. Bold letters and numbers correspond to position labels in Tables 1 and 2. Non-bolded numbers indicate chemical shifts in ppm. Dashed arrows indicate HMBC interactions.

The ^{1}H and ^{13}C NMR data for **6a** and **6d** also clearly indicated the presence of two methoxy groups, each of which was positioned on an aliphatic methyne (eventually established as C1 and C6). The presence of the methoxy groups was further established by the high resolution mass spectrum for **6d** (ESI-HRMS; calculated for

[M+Na]$^+$: 603.3234, found: 603.3233), which included a notable fragmentation peak of M^+=549.3152, indicating the loss of an OCH_3 group during the ionization process.

The accurate mass data, confirming a molecular formula of $C_{38}H_{36}O_2$ for **6a** and $C_{42}H_{44}O_2$ for **6d**, together with evidence from the NMR data,[29–33] allowed us to establish the core of **6** as being a tricyclo[5.2.1.$0^{2,6}$]decane, in which the *endo* linkage at the C3a/C7a ring fusion is a legacy of the original Diels–Alder reaction that produced the Thiele's ester intermediate from which **1a** and **1b** were derived. Coupling patterns observed throughout the ^{1}H NMR, such as the characteristic signals for the apical methylene group connected to two bridgehead methynes,[17] along with COSY and HMBC correlations as discussed below were coupled with mechanistic considerations to elaborate the core of the structure.

Working inward from the two 1,1-diarylalkene fragments, we found that we could conveniently divide the spin systems of the tricyclo[5.2.1.$0^{2,6}$]decane core into two sets (labeled in orange and blue, respectively, in Tables 1 and 2), since the constrained dihedral angles in the vicinity of the bridgehead protons H4 and H7 limited coupling between the Western and Eastern halves of the molecule.

Table 1. Chemical Shift Assignments for 6a in $CDCl_3$.

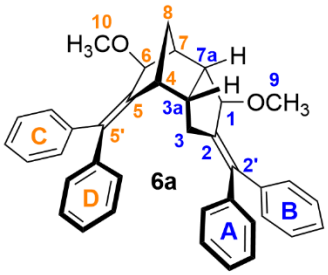

#	^{1}H	^{13}C	#	^{1}H	^{13}C
4	3.01	46.01	1	4.39	82.88
5	-	142.06	2	-	142.10
5'	-	139.39	2'	-	137.94
6	4.23	79.76	3	2.30/2.77	33.44
7	2.57	44.32	3a	2.66	44.06
8	1.44/1.91	38.21	7a	2.56	49.63
10	2.94	57.74	9	2.94	56.07

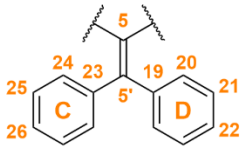

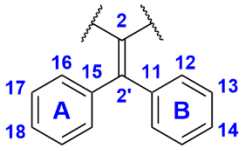

#	^{1}H	^{13}C	#	^{1}H	^{13}C
19	-	142.77	11	-	142.99
20	6.65-6.67	129.42	12	7.42-7.43	129.84
21	7.11-7.12	128.15	13	7.38-7.40	130.21
22	7.11-7.12	126.35	14	7.32-7.35	126.92
23	-	142.74	15	-	143.86
24	7.24-7.25	127.74	16	7.32-7.35	127.03
25	7.19-7.20	127.58	17	7.38-7.40	128.03
26	7.14-7.15	126.42	18	7.24-7.25	128.79

Table 2. Chemical Shift Assignments for 6d in Acetone-d6.

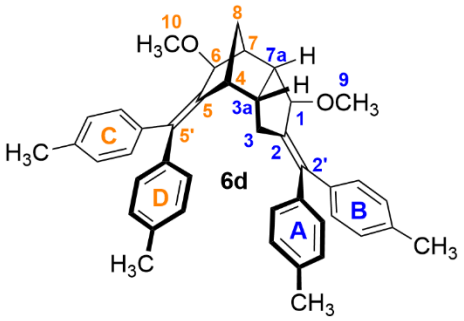

#	^1H	^{13}C	#	^1H	^{13}C
4	2.94	46.09	1	4.37	82.25
5	-	141.51	2	-	143.09
5'	-	138.40	2'	-	137.20
6	4.25	79.28	3	2.30/2.65	33.08
7	2.59	43.99	3a	2.62	43.80
8	1.39/1.81	37.50	7a	2.55	49.42
10	2.92	56.63	9	2.91	54.74

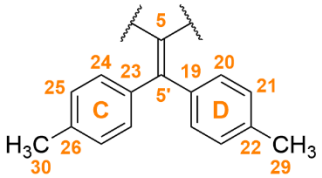

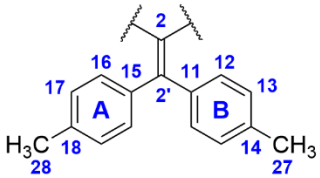

#	^1H	^{13}C	#	^1H	^{13}C
19	-	135.52	11	-	136.13
20	6.55	129.19	12	7.32	129.57
21	6.97	128.66	13	7.25	128.72
22	-	140.37	14	-	140.21
23	-	135.35	15	-	136.30
24	7.10	128.54	16	7.21	129.95
25	7.01	127.73	17	7.09	128.03
26	-	140.10	18	-	139.67
29	2.25	20.21	27	2.38	20.27
30	2.27	20.23	28	2.27	20.23

Many key assignments in **6a** and **6d** were made based upon HMBC correlations of carbinol protons H1 (a singlet) and H6 (a doublet) with nearby carbons (Figure 5). The signal corresponding to H1 correlated to the resonance for C9, the methoxy substituent attached to C1. Additional correlations to methylene C3 and bridgehead C3a indicated that H1 and C1 (and therefore the C9 methoxy group) were located on the Eastern cyclopentane ring of the tricycle. Further correlation between H1 and C2' situated the aryl groups A and B (and thus the 1,1-diarylalkene fragment in which they are included) within the *endo*-cyclopentane motif, adjacent to

C1. Selective pulsing at the frequency for H1 (4.4 ppm) in a 1D NOE experiment revealed spin polarization transfer to H12, the *ortho* proton of aromatic ring B (Figure S21). This allowed us to establish the geometry of the Eastern alkene, with aryl ring B being oriented *syn* to C1.[33] There was also an observable NOE interaction between H1 and bridgehead proton H7, indicating that the H1 proton faces inward toward the core of the molecule. This confirmed that the stereochemistry at C1 places the methoxy group into an *exo* orientation.

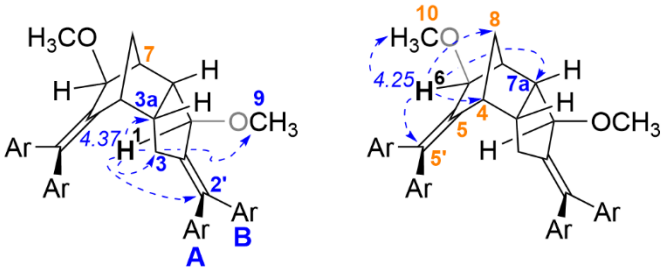

Figure 5. Key HMBC correlations from carbinol protons H1 and H6 establish connectivity within the molecule.

Similarly, HMBC correlation of the signal from H6 to that of the bridging methylene at C8 situated the carbinol centre C6 within the Western half of the molecule, allylic to C5. Correlations to resonances at C5 and C5' placed aryl substituents C and D (and thus the 1,1-diarylalkene fragment in which they are included) adjacent to C6, although selective pulsing of the signal for H6 in a 1D NOE experiment did not reveal the geometry of the alkene. The ^{2}J cross-peak observed between H6 and C5 in the HMBC spectrum may arise from initial spin transfer between H6 and C4, which was another correlation observed within the HMBC data.[31,32] Finally, an HMBC correlation between carbinol proton H6 and bridgehead carbon C7a was critically important in assigning the C10 methoxy group regiochemistry as being adjacent to C7, which left the 1,1-alkylidene group as being connected to C4; assignments of C3a and C7a were made clearer when looking at correlations to the signals corresponding to the bridging methylene protons H8 and H8' (*vide infra*).

The initial assignment of H8 and H8' was made based upon their coupling to one another (^{2}J = 9.3 Hz), and their lack of coupling to the bridgehead protons H4 and H7—something that is common for bicyclo[2.2.1]heptane systems due to the *ca.* 90° dihedral angle between the protons of the apical methylene

group and the bridgehead hydrogens.[34] A ^{1}H–^{1}H correlation between H8 and H6 observed in the COSY spectrum also informed upon the stereochemistry of the carbinol centre at C6 (Figure 6). Specifically, the 1.8 Hz ^{4}J coupling (W-coupling)[34,35] indicated the relative geometry of H6 relative to the rest of the molecule, which in turn established that the C10 methoxy group was in an *exo* orientation.

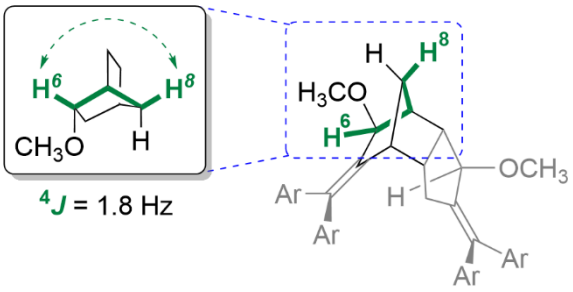

Figure 6. COSY correlation between H6 and H8, consistent with a ^{4}J coupling frequency of 1.8 Hz. The W-shape of the bonds between H6 and H8 is highlighted in green.

The ^{4}J coupling between H6 and H8 was visible in the COSY spectra for both **6a** and **6b**, but due to peak broadening H6 appeared as a broad singlet in the ^{1}H NMR spectrum for **6d**. In the ^{1}H NMR spectrum for **6a** the peak corresponding to H6 appeared as a narrow doublet.

The W-coupling between H6 and H8 also allowed us to differentiate H8 and H8', with the former pointing toward the *endo*-cyclopentane motif. As shown in Figure 7, H8 showed HMBC correlations to C5 and C6, while H8' correlated to C3a and C7a. Correlation of the signal for H8 to that of C5 confirmed the placement of the 1,1-diarylalkene motif containing rings C and D in the Western half of the molecule.

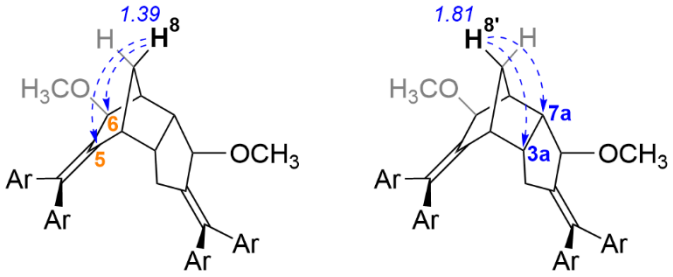

Figure 7. HMBC correlations for H8 and H8'.

Additional evidence in support of the assigned structure for **6a** and **6b** came by examining HMBC correlations from bridgehead protons H3a and H7a (Figure 8), as well as HMBC and NOE correlations for the diastereotopic methylene protons at C3 (Figure 9). For H3a, there was a strong HMBC cross-peak observed to the C2 resonance, with weaker ^{3}J correlations to resonances of C1 and C5, perhaps from poor spin transfer interactions due to the bond angles of the bridgehead C–H bonds.[36] There were also observable ^{2}J correlations in the HMBC spectra, from the signal for H3a to the resonances for C3, C4, and C7a. The signal for H3a appears as a triplet of doublets in the ^{1}H NMR, borne from coupling to protons H3/H3', H4, and H7a. The strong ^{1}H–^{1}H coupling likely results in an enhanced ^{2}J correlation signal in the HMBC spectra from the respective carbons to H3a through spin polarization transfer.[31,32] The HMBC correlations for H7a were largely ^{3}J, with correlations observed to resonances for C2, C3, C4, and C6, as well as a ^{2}J correlation to the resonance for C1. The correlations from H3a and H7a to the carbons of the Eastern half of the molecule unambiguously place the two protons at the bridgehead positions adjacent to C4 and C7, respectively.

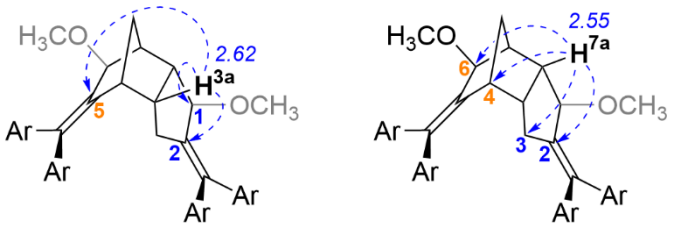

Figure 8. HMBC correlations for H3a and H7a.

The methylene protons *endo*-H3 and *exo*-H3' displayed key correlations in the HMBC spectra that positioned C4 between carbons C3a and C5. Correlations from the signal for H3 to those of C1, C2', C4, and C7a helped to solidify the assignments already made on the Eastern half of the molecule. Correlations from the signal for H3' to those of C2' and C4 were likewise observed, alongside ^{2}J correlation to the resonances for C3a and C2. These ^{2}J correlations to C3a and C2 were observed for H3 as well. From the 1D NOE spectra for H3 (Figure S24), through-space correlation of the signals for H3 and H4 positioned both protons within proximity of one another (hence the *endo* assignment for H3). Small NOE correlations to carbinol protons H1 and H6 were also observed, further confirming the assignment of the *exo*,*exo*-diastereomer **6a**/**6d**. There were also notable NOE correlations from H3 to H16 (the *ortho*-proton of aryl ring A) and to H20 (the *ortho*-proton of aryl ring D) which informed the placement of these two rings relative to the dicyclopentadienyl core of the molecule, and finally established the geometry of the Western 1,1-diarylalkene.

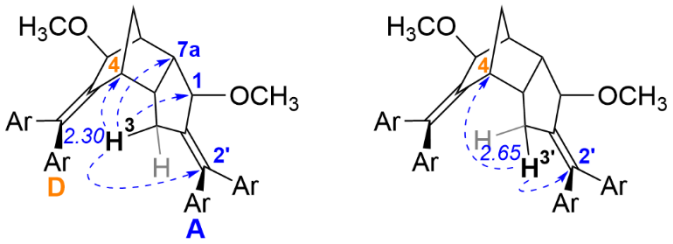

Figure 9. HMBC correlations for H3 and H3'.

Finally, the HMBC correlations for bridgehead protons H4 and H7 are shown in Figure 10. The signal for H4 exhibited correlations to the resonances for C5', C6 and C7a, comfortably situating H4 three bonds away from each carbon at the norbornane bridgehead position. Correlation of the resonance for H7 to that of C1 placed it opposite to C4. Both of the signals for H4 and H7 also exhibited ^{3}J correlations to the carbon resonance bearing the opposite proton (i.e. H4 to C7 and *vice versa*), further confirming their positions at the bridgehead carbon centres.

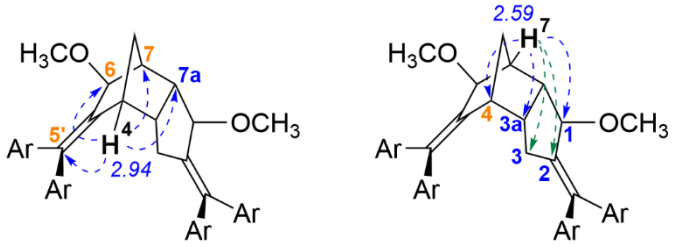

Figure 10. HMBC correlations for H4 and H7a. ^{4}J couplings are indicated in green.

In contrast to the extended pinacol product **2**, for which *either* stepwise *or* concerted pathways could in principle be responsible for production of the observed product, the structure of compound **6** implies a stepwise mechanism proceeding through two sequential ring-openings (Scheme 4). The proposed mechanism begins by protonation of diol **1** and subsequent loss of water to form equilibrating cations **I** and **II** (as discussed above; additional evidence for this equilibration was afforded by the isolation and characterization of tetrahydrofuran **7**, the free base of proposed intermediate **III**, during a reaction using **1a**). Ring-opening of the strained cyclobutane bond in **I** and **II** (between C2 and C5) leads to regioisomeric 3° carbocations **IV** and **V**—intermediates that are unlikely to interconvert on the timescale of the reaction, since doing so (through a Prins-type reaction to reform **I** and **II**) would require reformation of the strained cyclobutane.

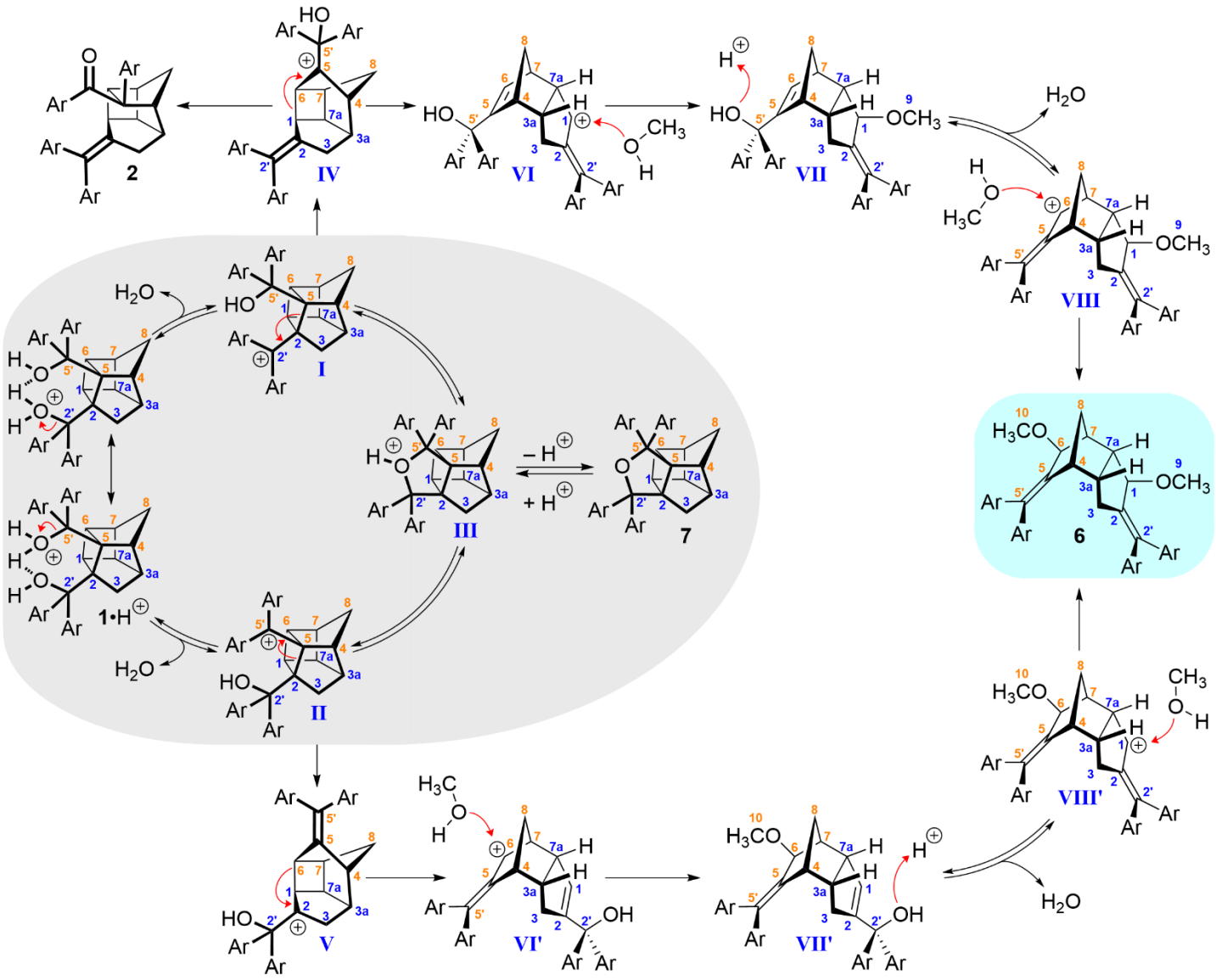

Scheme 4. Proposed mechanism for the production of side product **6** from cations **IV** and **V**.

As illustrated in Scheme 4, however, either **IV** or **V** could undergo ring-opening of a second cyclobutane bond (this time between C1 and C6) to result in a new pair of resonance-stabilized benzylic cations, **VI** and **VI'**. Indeed, the proposed conversion from **IV** to **VI** (or from **V** to **VI'**) would hardly be surprising in light of similar fragmentations reported for analogous cyclobutylcarbinyl cations.[37] Benzylic cations **VI** and **VI'** could suffer the addition of methanol (from the solvent) at C1 or C6, respectively, leading to intermediates **VII** and **VII'**, which still contain a reactive allylic alcohol. Each of these intermediates could undergo protonation and subsequent loss of water to form a new resonance-stabilized benzylic cation (**VIII** or **VIII'**), which would in turn suffer an additional attack by methanol to afford the observed rearrangement product, **6**. In both cases the methanol

would preferentially approach the carbocation *exo* to the tricyclic core, leading to the observed stereochemistry at the two carbinol centres in the product.

The mechanistic implications engendered by the isolation of **6** are significant. Because **6** almost certainly arises from a series of carbocation intermediates (the formation of methanol adducts is strong evidence for this), the existence of **6** provides direct evidence for the production of carbocations from diol **1**, which in turn constitutes experimental evidence favoring a stepwise pathway leading to the extended pinacol product, **2**. Moreover, the experimental observation of **6** under the conditions used for the alkyl-extended pinacol rearrangement finally answers the question of what happens to material that passes through intermediate **V**: instead of rearranging *via* a 1,2-aryl shift to afford **4** or **5**, it undergoes cleavage of a second cyclobutane bond to eventually form compound **6**.

A holistic mechanistic picture thus begins to emerge from our studies. Thiele cage diol **1** begets the equilibrating mixture of cations **I** and **II** following protonation and loss of water. These species in turn undergo ring-opening to afford **IV** and **V**, at which point the two possible reaction pathways begin to differ. It is likely that most of the material that passes through **IV** undergoes immediate 1,2-aryl shift (possibly through the intermediacy of a spirocyclopropylarenium ion) to afford pinacol product **2**. Both the rate of this reaction and the stereochemical outcome are influenced by the fact that one arene ring is positioned appropriately to undergo migration. We can thus surmise that **IV** must be a short-lived intermediate, and that the conformational preferences of the starting material govern the reaction pathway. The substituents on intermediate **V**, on the other hand, are not appropriately positioned to support a fast 1,2-aryl migration. Any material passing through **V** therefore undergoes a second cyclobutane ring-opening leading to product **6**.

Conclusion

A side product observed during the alkyl-extended pinacol rearrangement of Thiele cage diol **1** into ketone **2** was isolated and characterized for the first time. The structure of the side product, **6**, implies the formation of carbocation intermediates under the reaction conditions, which provides important evidence in favour of a

stepwise carbocation pathway leading to **2**. Of the regioisomeric carbocation intermediates that can be generated by ring-opening in **1**, it is likely that one carbocation (**IV**) leads exclusively to **2** *via* a fast 1,2-aryl migration, while the other (**V**) leads to **6** through a secondary ring-opening event.

Acknowledgements

Financial support as provided by the Natural Sciences and Engineering Research Council of Canada (NSERC) through a Discovery grant to J.W. The authors also thank NSERC for a fellowship to J.S. and Prof. Gino DiLabio for helpful discussions.

Author information

Author ORCIDs

Jeremy E. Wulff https://orcid.org/0000-0001-9670-160X

Author contributions

Formal Analysis: A.B., J.S., J.W.

Investigation: A.B., J.S.

Methodology: A.B., J.S.

Funding acquisition: J.W.

Project administration: J.W.

Writing – original draft: A.B.

Writing – review & editing: A.B., J.S., J.W.

Competing interests

The authors declare that there are no competing interests.

Supplementary material

Supplementary data are available with the article at: https//doi.org/xxxx

Experimental

General procedures. All reactions were performed in flame-dried glassware equipped with rubber septa under an inert argon atmosphere. Organic solutions were concentrated at 30 to 50°C *in vacuo* by rotary evaporation. THF was freshly distilled over sodium and benzophenone. Organometallic reagents were purchased from Sigma-Aldrich and were used as received. Solvents and air-sensitive solutions were transferred via stainless-steel cannula or via plastic syringe equipped with a stainless-steel needle. Thin layer chromatography was performed on MACHEREY-NAGEL pre-coated ALUGRAM® SILG/UV_{254} TLC plates (0.20 mm silica gel 60 with 254 nm fluorescent indicator). TLC plates were visualized under UV light (254 nm) and developed by staining and heating with $KMnO_4$. Flash column chromatography was performed on silica gel (60 Å, 40-63 µm, Silicycle SiliaFlash® F60).

NMR spectra for characterization were recorded at ambient temperature (298 K). ^1H NMR and ^{13}C NMR spectra for compounds **1d**, **6a**, **6d** and **7a** were recorded at 500 and 126 MHz, respectively, on a Bruker AVANCE NEO 500 spectrometer equipped with a BBF probe. The ^1H and ^{13}C NMR spectra for compound **1a** were recorded at 300 and 76 MHz, respectively, on a Bruker AVANCE 300 spectrometer equipped with a 5 mm QNP probe. ^1H chemical shifts (δ) are reported in parts-per-million (ppm) relative to tetramethylsilane and referenced to the solvent peak ($CDCl_3$, δ 7.26; CD_2Cl_2, δ 5.32; $(CD_3)_2CO$, δ 2.05). NMR data is presented as follows: chemical shift, multiplicity (s = singlet, d = doublet, dd = doublet of doublets, t = triplet, q = quartet, m = multiplet, tdd = triplet of doublet of doublets, bs = broad singlet, app = apparent), coupling constants (*J*, reported in Hz), integration. All ^{13}C-NMR spectra are proton-decoupled ($^{13}C\{^1H\}$). ^{13}C chemical shifts (δ) are reported in parts-per-million (ppm) relative to tetramethylsilane and referenced to the solvent peak ($CDCl_3$, δ 77.16; CD_2Cl_2, δ 53.84; $(CD_3)_2CO$, δ 29.84). Prior to recording NOESY spectra, samples were sparged by bubbling argon through the NMR tube for several minutes. Infrared spectra were obtained using a Perkin-Elmer ATR spectrometer and a Perkin-

Elmer FTIR Spectrometer Two via thin film on a salt (NaCl) plate. IR wavenumbers (ν) are reported cm^{-1}. Accurate masses were obtained by electrospray ionization high-resolution mass spectrometry (HRMS) using a Thermo Scientific™ Exactive™ Plus Orbitrap Ultimate 3000 LC-MS system. Melting points were measured using a Gallenkamp melting point apparatus and are uncorrected.

Preparation of Thiele cage diols. A flame-dried round bottom flask under inert Ar atmosphere was charged with the Thiele cage methyl ester and THF (to a concentration of 0.07 to 0.10 M; typically, 0.36 mmol in 4 mL THF). To this solution was added the appropriate commercial organometallic reagent solution at 0°C dropwise over 5 minutes. The reaction mixture was warmed to room temperature overnight (14 hours), then cooled to 0°C. The mixture was quenched with the addition of saturated solution of NH_4Cl (5 mL) and diluted with distilled water (5 mL) and Et_2O (10 mL). The two phases were separated, and the aqueous phase was the extracted with Et_2O (3 x 10 mL). The combined organic phases were washed with brine (1 x 20 mL), dried over Na_2SO_4, then concentrated *in vacuo* to afford the crude diol as a foamy solid. Each diol was purified via flash-column chromatography with hexanes/ethyl acetate as the eluent.

Diol 1a. Prepared according to the procedure by Dao *et al.*[16] following the general procedure above, using commercial (Sigma-Aldrich) phenyllithium solution (1.8 M in dibutyl ether). Spectral details matched those reported in the literature.[16] ^{1}H NMR (300 MHz, $CDCl_3$): δ 7.40-7.36 (m, 2H), 7.24-6.95 (m, 15H), 6.83-6.78 (m, 3H), 4.65 (bs, 1H), 4.25 (bs, 1H), 3.51-3.46 (m, 1H), 3.15-3.11 (m, 1H), 3.08-3.03 (m, 1H),2.74-2.62 (m, 2H), 2.57-2.54 (m, 1H), 2.47-2.44 (m, 1H), 2.08 (d, *J* = 11.8 Hz, 1H), 0.96 (d, *J* = 11.3 Hz, 1H), −0.65 (d, *J* = 11.3 Hz, 1H); ^{13}C NMR (75 MHz, $CDCl_3$): δ 147.5, 147.2, 146.8, 145.7, 128.1, 127.9, 127.6, 127.3, 127.0, 126.9, 126.8, 126.7, 126.3, 80.4, 80.4, 70.2, 68.8, 53.9, 47.3, 42.7, 42.4, 40.9, 38.9, 38.3; IR (film): 3390, 3057, 2973, 1639, 1493, 1446 cm^{-1}.

Diol 1d. Prepared according to the general procedure above, using commercial (Sigma-Aldrich) 4-tolylmagnesium bromide solution (1.0 M in THF). The product was purified by flash-column chromatography, eluting with hexanes:EtOAc 10:1, to afford the desired product as a white solid (200 mg, 0.362 mmol, 56% yield). M.p. 183–184 °C; ^{1}H NMR (500 MHz, CD_2Cl_2): δ 7.26 (d, *J* = 8.4 Hz, 2H), 7.08-7.03 (m, 6H), 6.92-6.86 (m, 4H), 6.81 (d, *J* = 8.0 Hz, 2H), 6.62 (d, *J* = 8.0 Hz, 2H), 4.46 (s, 1H), 4.32 (s, 1H), 3.42-3.39 (m, 1H), 3.04-3.00 (m, 2H), 2.64-2.60 (m, 2H), 2.52-2.51 (m, 1H), 2.42-2.41 (m, 1H), 2.31 (s, 3H), 2.27 (s, 3H), 2.22 (s, 3H), 2.15 (s, 3H), 0.94 (d, *J* = 11.1 Hz, 1H), −0.59 (d, *J* = 11.1 Hz, 1H); ^{13}C NMR (126MHz, CD_2Cl_2): δ 145.1, 144.9, 144.7, 143.8, 136.9, 135.7, 128.8, 128.6, 128.4, 128.3, 128.3, 128.1, 128.0, 127.2, 80.3, 80.2, 47.6, 44.7, 43.1, 42.5, 41.2, 39.4, 38.8, 21.3, 21.1, 21.1, 21.1; IR (film): 3536, 3245, 3025, 2970, 2921, 1508, 807 cm^{-1}; HRMS (ESI+): *m/z* calcd. for $C_{40}H_{40}O_2Na$ $[M + Na]^+$ 575.2921, found 575.2925.

Rearrangement product 6a. To a 20-mL scintillation vial containing a solution of **1a** (52.1 mg, 0.105 mmol) in methanol (3.0 mL) was added concentrated sulfuric acid (14.0 μL, 0.263 mmol). Upon addition of acid, the mixture became yellow, then quickly became colourless again. After 2.5 minutes, more methanol (0.5 mL) was added and the reaction was placed into a pre-heated oil bath at 43°C while stirring with the vial loosely capped. The reaction was stirred for 2 hours 50 minutes and cooled to room temperature before quenching with a large excess (*ca.* 250 mg) of K_2CO_3 while stirring for an additional 10 minutes. The mixture was filtered through cotton and washed with small volumes of MeOH and EtOAc, then concentrated to a crude, off-white solid (72.2 mg). The product was purified via flash-column chromatography (gradient eluent – hexanes:EtOAc 20:1 – 10:1 – 5:1) to provide a white solid (5 mg, 0.010 mmol, 9% yield). M.p. 173–175 °C; ^{1}H NMR (500 MHz, $CDCl_3$): δ 7.43-7.42 (m, 2H), 7.40-7.38 (m, 3H), 7.35-7.32 (m, 3H), 7.25-7.24 (m, 3H), 7.20-7.18 (m, 2H), 7.16-7.13 (m, 1H), 7.13-7.10 (m, 3H), 6.68-6.64 (m, 2H), 4.39 (s, 1H), 4.24 (d, *J* = 1.6 Hz, 1H), 3.01 (d, *J* = 4.4 Hz, 1H), 2.94 (s, 3H), 2.94 (s, 3H), 2.77 (dd, *J* = 17.5, 10.2 Hz, 1H), 2.66 (tdd, *J* =10.1, 4.9, 1.5 Hz, 1H), 2.60 (d, *J* = 5.0 Hz, 1H), 2.56 (dd, *J* = 10.4, 5.2 Hz, 1H), 2.30 (d, *J* = 17.5 Hz, 1H), 1.91 (d, *J* = 9.6 Hz, 1H), 1.44 (d, *J* = 9.2 Hz, 1H); ^{13}C NMR (126 MHz, $CDCl_3$): δ 143.9, 143.0, 142.9, 142.7, 142.1, 142.1, 139.4, 137.9, 130.2, 129.8, 129.4, 128.8, 128.3, 128.2, 127.7, 127.6,

127.0, 126.9, 126.4, 126.4, 82.9, 79.8, 54.7, 56.1, 49.6, 46.0, 44.3, 44.06, 38.2, 33.4; IR (film): 3057, 3024, 2926, 2815, 1599, 1492, 1443 cm^{-1}; HRMS (ESI+): *m/z* calcd. for $C_{38}H_{36}O_2Na$ $[M + Na]^+$ 547.2607, found 547.2607.

Rearrangement product 6d. To a 20-mL scintillation vial containing a solution of **1d** (261 mg, 472 mmol) in methanol (5.0 mL) was added sulfuric acid (100 µL, 1.88 mmol) in a solution of methanol (1 mL). The mixture was heated at 40°C overnight for 16 hours, then cooled to 0°C and quenched with saturated $NaHCO_3$ solution to afford a neutral solution. The mixture was diluted with water (5 mL) and Et_2O (5 mL), then the two phases were separated, and the aqueous layer was further extracted with Et_2O (2 x 5 mL). The combined organic phase was dried with anhydrous sodium sulfate, filtered, then concentrated *in vacuo* to afford a crude yellow solid (308 mg). The crude material was purified via flash-column chromatography (hexanes:EtOAc 4:1) and subsequent preparative TLC (hexanes:EtOAc 1:1) to provide **6d** as a white solid (35.1 mg, 60.4 mmol, 13% yield). ^1H NMR (500 MHz, $(CD_3)_2CO$): δ 7.32 (d, *J* = 8.1 Hz, 2H), 7.28 (d, *J* = 7.8 Hz, 2H), 7.21 (d, *J* = 8.2 Hz, 2H), 7.10 (d, *J* = 8.5 Hz, 2H), 7.01 (d, *J* = 7.9 Hz, 2H), 6.97 (d, *J* = 7.8 Hz, 2H), 6.55 (d, *J* = 8.0 Hz, 2H), 4.37 (s, 1H), 4.25 (d, *J* = 2.0 Hz, 1H), 2.94 (d, 1H), 2.92 (s, 3H), 2.91 (s, 3H), 2.67-2.54 (m, 4H), 2.38 (s, 3H), 2.32 (s, 3H), 2.27 (s, 3H), 2.25 (s, 3H), 1.81 (d, *J* = 9.3 Hz, 1H), 1.39 (d, *J* = 9.3 Hz, 1H); ^{13}C NMR (126 MHz, $(CD_3)_2CO$): δ 143.1, 141.5, 140.4, 140.2, 140.1, 139.7, 138.4, 137.2, 136.3, 136.1, 135.5, 135.4, 130.0, 129.6, 129.2, 128.7(72), 128.7(66), 128.5, 128.0, 127.7, 82.3, 79.3, 56.6, 54.7, 49.4, 46.1, 44.0, 43.8, 37.5, 33.1, 20.3, 20.2(23), 20.2(23), 20.2(21); HRMS (ESI+): *m/z* calcd. for $C_{42}H_{44}O_2Na$ $[M + Na^+]^+$ 603.3234, found 603.3233.

Tetrahydrofuran 7a. Compound **7a** (the free base of proposed intermediate **III**) was isolated by flash-column chromatography from a reaction of **1a** that also afforded **2a** and **6a**. R_f = 0.66 (9:1 petroleum ether : Et_2O). M.p. 207–211 °C ; ^1H NMR (500 MHz, $CDCl_3$): δ 7.45 (app d, *J* = 7.3 Hz, 2H), 7.42-7.38 (m, 6H), 7.32-7.27 (m, 2H), 7.21 (m, 1H), 7.10-7.03 (m, 8H), 7.00 (m, 1H), 2.83-2.80 (m, 1H), 2.65-2.59 (m, 2H), 2.52-2.50 (m, 1H), 2.14-2.12 (m, 2H), 2.00 (d, *J* = 10.9 Hz, 1H), 1.88 (d, *J* = 10.9 Hz, 1H), 1.75 (d, *J* = 11.5 Hz, 1H), 1.47 (d, *J* = 11.5 Hz, 1H); ^{13}C NMR (126 MHz, $CDCl_3$): δ 148.38, 148.33, 146.96, 144.99, 128.76, 127.82, 127.73, 127.65, 127.59, 127.54, 127.43,

126.57, 126.43, 126.35, 126.18, 125.72, 91.45, 89.62, 71.34, 71.27, 51.33, 50.96, 45.80, 42.76, 41.29, 40.76, 39.84, 38.11; IR (film): 3058, 2979, 2864, 1600, 1490, 1446, 1023, 699 cm^{-1}; HRMS (ESI+): *m/z* calcd. for $C_{36}H_{31}O$ $[M + H]^+$ 479.2370, found 479.2370.

References

(1) Fittig, R. 41. Ueber Einige Derivate Des Acetons. *Justus Liebigs Ann. Chem.* **1860**, *114* (1), 54–63. https://doi.org/10.1002/jlac.18601140107.

(2) Butlerow, A. Ueber Trimethylessigsäure. *Justus Liebigs Ann. Chem.* **1873**, *170* (1–2), 151–162. https://doi.org/10.1002/jlac.18731700114.

(3) Song, Z.-L.; Fan, C.-A.; Tu, Y.-Q. Semipinacol Rearrangement in Natural Product Synthesis. *Chem. Rev.* **2011**, *111* (11), 7523–7556. https://doi.org/10.1021/cr200055g.

(4) Gao, A. X.; Thomas, S. B.; Snyder, S. A. Pinacol and Semipinacol Rearrangements in Total Synthesis. In *Molecular Rearrangements in Organic Synthesis*; John Wiley & Sons, Ltd, 2015; pp 1–34. https://doi.org/10.1002/9781118939901.ch1.

(5) Pettit, G. R.; Lippert, J. W.; Herald, D. L. A Pinacol Rearrangement/Oxidation Synthetic Route to Hydroxyphenstatin. *J. Org. Chem.* **2000**, *65* (22), 7438–7444. https://doi.org/10.1021/jo000705j.

(6) Suzuki, K.; Takikawa, H.; Hachisu, Y.; Bode, J. W. Isoxazole-Directed Pinacol Rearrangement: Stereocontrolled Approach to Angular Stereogenic Centers. *Angew. Chem. Int. Ed.* **2007**, *46* (18), 3252–3254. https://doi.org/10.1002/anie.200605138.

(7) Wu, H.; Wang, Q.; Zhu, J. Catalytic Enantioselective Pinacol and Meinwald Rearrangements for the Construction of Quaternary Stereocenters. *J. Am. Chem. Soc.* **2019**, *141* (29), 11372–11377. https://doi.org/10.1021/jacs.9b04551.

(8) Snyder, S. A.; Thomas, S. B.; Mayer, A. C.; Breazzano, S. P. Total Syntheses of Hopeanol and Hopeahainol A Empowered by a Chiral Brønsted Acid Induced Pinacol Rearrangement. *Angew. Chem. Int. Ed.* **2012**, *51* (17), 4080–4084. https://doi.org/10.1002/anie.201107730.

(9) Jørgensen, L.; McKerrall, S. J.; Kuttruff, C. A.; Ungeheuer, F.; Felding, J.; Baran, P. S. 14-Step Synthesis of (+)-Ingenol from (+)-3-Carene. *Science* **2013**, *341* (6148), 878–882. https://doi.org/10.1126/science.1241606.

(10) He, C.; Xuan, J.; Rao, P.; Xie, P.-P.; Hong, X.; Lin, X.; Ding, H. Total Syntheses of (+)-Sarcophytin, (+)-Chatancin, (−)-3-Oxochatancin, and (−)-Pavidolide B: A Divergent Approach. *Angew. Chem. Int. Ed.* **2019**, *58* (15), 5100–5104. https://doi.org/10.1002/anie.201900782.

(11) Lutz, R. E.; Bass, R. G.; Boykin, D. W. Jr. Rearrangement of the Vinylog of Benzpinacol. *J. Org. Chem.* **1964**, *29* (12), 3660–3664. https://doi.org/10.1021/jo01035a057.

(12) Saito, K.; Horie, Y.; Mukai, T.; Toda, T. The Pyrolyses of 1,1,4,4,-Tetraphenyl-1,4-Butanediol and 1,1,4,4-Tetraphenyl-2-Butene-1,4-Diol Derivatives. Decomposition Reactions to Form Olefins via the Elimination of Two Mole Equivalents of the Hydroxydiphenylmethyl Radical. *Bull. Chem. Soc. Jpn.* **1985**, *58* (11), 3118–3124. https://doi.org/10.1246/bcsj.58.3118.

(13) Zhu, L.; Li, X.-X.; Zhou, W.; Li, X.; Chen, Z. Divergent Synthetic Routes for Ring Expansion or Cyclization from 1,4-Allylic Diol Derivatives via Gold(I) Catalysis or Zinc(II) Mediation. *J. Org. Chem.* **2011**, *76* (21), 8814–8823. https://doi.org/10.1021/jo2015517.

(14) Wu, H.; Wang, Q.; Zhu, J. Organocatalytic Enantioselective Vinylogous Pinacol Rearrangement Enabled by Chiral Ion Pairing. *Angew. Chem. Int. Ed.* **2016**, *55* (49), 15411–15414. https://doi.org/10.1002/anie.201609911.

(15) Darby, R. A.; Lutz, R. E. Pinacollike Rearrangement of a Cyclopropane-1,2-Dimethylene Glycol. *J. Org. Chem.* **1957**, *22* (11), 1353–1355. https://doi.org/10.1021/jo01362a014.

(16) Dao, N.; Sader, J. K.; Oliver, A. G.; Wulff, J. E. Prying Open a Thiele Cage: Discovery of an Unprecedented Extended Pinacol Rearrangement. *Chem. Commun.* **2019**, *55* (11), 1600–1603. https://doi.org/10.1039/C8CC08862D.

(17) Chen, J.; Kilpatrick, B.; Oliver, A. G.; Wulff, J. E. Expansion of Thiele's Acid Chemistry in Pursuit of a Suite of Conformationally Constrained Scaffolds. *J. Org. Chem.* **2015**, *80* (18), 8979–8989. https://doi.org/10.1021/acs.joc.5b01332.

(18) Peters, D. 211. Simple Derivatives of Cyclopentadiene. Part IV. The Dimerisation of Methyl Cyclopentadiene-1-Carboxylate. *J. Chem. Soc.* **1961**, 1042–1048. https://doi.org/10.1039/JR9610001042.

(19) Dive, G.; Robiette, R.; Chenel, A.; Ndong, M.; Meier, C.; Desouter-Lecomte, M. Laser Control in Open Quantum Systems: Preliminary Analysis toward the Cope Rearrangement Control in Methyl-Cyclopentadienylcarboxylate Dimer. *Theor. Chem. Acc.* **2012**, *131* (6), 1236. https://doi.org/10.1007/s00214-012-1236-5.

(20) Chen, J.; Wulff, J. E. Revisiting the Mechanistic Origins of Thiele's Ester Dimerization: Probing the Reliability of Predictive Models for Cycloadditions. *Org. Biomol. Chem.* **2016**, *14* (43), 10170–10174. https://doi.org/10.1039/C6OB02218A.

(21) Dunn, G. L.; Donohue, J. K. The Structure of Thiele's Ester, a Dimethyl Dicyclopentadienedicarboxylate. *Tetrahedron Lett.* **1968**, *9* (31), 3485–3487. https://doi.org/10.1016/S0040-4039(01)99089-6.

(22) Marchand, A. P.; Zhao, D.; Ngooi, T.-K.; Vidyasagar, V.; Watson, W. H.; Kashyap, R. P. Thiele's Ester as a Reagent in Organic Synthesis. Preparation of Pentacyclo[5.4.0.02,5.03,10.04,8]Undecane-10-Carboxylic Acid. *Tetrahedron* **1993**, *49* (13), 2613–2620. https://doi.org/10.1016/S0040-4020(01)86340-7.

(23) Marchand, A. P.; Namboothiri, I. N. N.; Lewis, S. B.; Watson, W. H.; Krawiec, M. Thiele's Acid Revisited: Isolation and Characterization of Two Minor Products Formed by Carbonation of Cyclopentadienide Anion. *Tetrahedron* **1998**, *54* (42), 12691–12698. https://doi.org/10.1016/S0040-4020(98)00770-4.

(24) Rajkumar, S.; Choudhari, R. S.; Chowdhury, A.; Namboothiri, I. N. N. Synthesis and Pyrolysis Studies of Bis(Nitratomethyl)-1,3-Bishomocubane—A High-Energy High-Density Liquid. *Thermochimica Acta* **2013**, *563*, 38–45. https://doi.org/10.1016/j.tca.2013.03.044.

(25) Lal, S.; Mallick, L.; Rajkumar, S.; Oommen, O. P.; Reshmi, S.; Kumbhakarna, N.; Chowdhury, A.; Namboothiri, I. N. N. Synthesis and Energetic Properties of High-Nitrogen Substituted Bishomocubanes. *J. Mater. Chem. A* **2015**, *3* (44), 22118–22128. https://doi.org/10.1039/C5TA05380C.

(26) Thiele, J. Ueber Abkömmlinge Des Cyclopentadiëns. *Ber. Dtsch. Chem. Ges.* **1901**, *34* (1), 68–71. https://doi.org/10.1002/cber.19010340114.

(27) Ziegler, K.; Froitzheim-Kühlhorn, H.; Hafner, K. Metallorganische Verbindungen XXI: Metallverbindungen des Cyclopentadiens. *Chem. Ber.* **1956**, *89* (2), 434–443. https://doi.org/10.1002/cber.19560890238.

(28) Doddrell, D. M.; Pegg, D. T.; Bendall, M. R. Distortionless Enhancement of NMR Signals by Polarization Transfer. *J. Magn. Reson.* **1982**, *48* (2), 323–327. https://doi.org/10.1016/0022-2364(82)90286-4.

(29) Hurd, R. E. Gradient-Enhanced Spectroscopy. *J. Magn. Reson.* **1990**, *87* (2), 422–428. https://doi.org/10.1016/0022-2364(90)90021-Z.

(30) Bodenhausen, G.; Ruben, D. J. Natural Abundance Nitrogen-15 NMR by Enhanced Heteronuclear Spectroscopy. *Chem. Phys. Lett.* **1980**, *69* (1), 185–189. https://doi.org/10.1016/0009-2614(80)80041-8.

(31) Bax, A.; Summers, M. F. Proton and Carbon-13 Assignments from Sensitivity-Enhanced Detection of Heteronuclear Multiple-Bond Connectivity by 2D Multiple Quantum NMR. *J. Am. Chem. Soc.* **1986**, *108* (8), 2093–2094. https://doi.org/10.1021/ja00268a061.

(32) Willker, W.; Leibfritz, D.; Kerssebaum, R.; Bermel, W. Gradient Selection in Inverse Heteronuclear Correlation Spectroscopy. *Magn. Reson. Chem.* **1993**, *31* (3), 287–292. https://doi.org/10.1002/mrc.1260310315.

(33) Stott, K.; Keeler, J.; Van, Q. N.; Shaka, A. J. One-Dimensional NOE Experiments Using Pulsed Field Gradients. *J. Magn. Reson.* **1997**, *125* (2), 302–324. https://doi.org/10.1006/jmre.1997.1110.

(34) Wemmer, D. E. Homonuclear Correlated Spectroscopy (COSY): The Basics of Two-Dimensional NMR. *Concepts Magn. Reson.* **1989**, *1* (2), 59–72. https://doi.org/10.1002/cmr.1820010204.

(35) Thomas, W. A. Unravelling Molecular Structure and Conformation—the Modern Role of Coupling Constants. *Prog. Nucl. Magn. Reson. Spectrosc.* **1997**, *30* (3), 183–207. https://doi.org/10.1016/S0079-6565(96)01033-3.

(36) Karplus, M. Vicinal Proton Coupling in Nuclear Magnetic Resonance. *J. Am. Chem. Soc.* **1963**, *85* (18), 2870–2871. https://doi.org/10.1021/ja00901a059.

(37) White, J. D.; Li, Y.; Kim, J.; Terinek, M. Cyclobutane Synthesis and Fragmentation. A Cascade Route to the *Lycopodium* Alkaloid (−)-Huperzine A. *J. Org. Chem.* **2015**, *80* (23), 11806–11817. https://doi.org/10.1021/acs.joc.5b01619.